

Coherence Time of a Solid-State Nuclear Qubit

T. D. Ladd,* D. Maryenko,† and Y. Yamamoto‡

*Quantum Entanglement Project, ICORP, JST, Edward L. Ginzton Laboratory,
Stanford University, Stanford, California 94305-4085, USA*

E. Abe and K. M. Itoh

*Department of Applied Physics and Physico-Informatics,
CREST, JST, Keio University, Yokohama, 223-8522, Japan*

(Dated: November 28, 2018)

We report NMR experiments using high-power, RF decoupling techniques to show that a ^{29}Si nuclear spin qubit in a solid silicon crystal at room temperature can preserve quantum phase for 10^9 precessional periods. The coherence times we report are longer than for any other observed solid-state qubit by more than four orders of magnitude. In high quality crystals, these times are limited by residual dipolar couplings and can be further improved by isotopic depletion. In defect-heavy samples, we provide evidence for decoherence limited by $1/f$ noise. These results provide insight toward proposals for solid-state nuclear-spin-based quantum memories and quantum computers based on silicon.

PACS numbers: 03.67.Lx, 03.67.Pp, 76.60.Lz, 82.56.Jn

Quantum information processing devices outperform their classical counterparts by preserving and exploiting the correlated phases of their constituent quantum oscillators, which are usually two-state systems called “qubits.” An increasing number of theoretical proposals have shown that such devices allow secure long-distance communication and improved computational power [1]. Solid-state implementations of these devices are favored for reasons of both scalability and integration with existing hardware, although previous experiments have shown limited coherence times for solid-state qubits. The development of quantum error correcting codes [2] and fault tolerant quantum computation [3] showed that large-scale quantum algorithms are still theoretically possible in the presence of decoherence. However, the coherence time must be dauntingly long: approximately 10^5 times the duration of a single quantum gate, and probably longer depending on the quantum computer architecture [1]. The question of whether a scalable implementation can surpass this coherence threshold is not only important for the technological future of quantum computation, but also for fundamental understanding of the border between microscopic quantum behavior and macroscopic classical behavior.

Experimentally observed coherence times (T_2) for various qubit implementations are shown in Table I. The atomic systems shown — trapped ions and molecular nuclei in liquid solution — have already been employed for small quantum algorithms [6, 13]; not coincidentally, they show very high values of Q , the product of the qubit frequency $\omega_0/2\pi$ and πT_2 . Most solid-state qubits show smaller values of Q ; as we demonstrate in this Letter, however, the long coherence times we observe in solid-state ^{29}Si nuclei afford them a Q and ΩT_2 as high or higher than atomic systems, indicating this system’s

promise for solid-state quantum computing.

Many promising qubits and coherence time measurements are not mentioned in Table I either because reliable experimental data are not available, or because the existing experimental data are taken under conditions not sufficiently similar to the corresponding quantum computer architecture. For example, electron spins bound to phosphorous donors in pure, isotopically depleted silicon also show promisingly long coherence times [14]. However, quantum computer architectures employing semiconductor electron qubits [15, 16] require semiconductor alloying and metallic nanostructures for wave-function engineering. These additions, rather than bulk phenomena, are likely to dominate decoherence for these qubits. Likewise, Kane has proposed an architecture for silicon-based quantum computing in which embedded ^{31}P nuclear spins are cooled, controlled, and measured with the engineered wave functions of donor electrons [17]. Charge fluctuations couple to the nuclei via the hyperfine interaction, leading to a nuclear decoherence source not necessarily observed in bulk experiments. However, we believe that bulk solid-state nuclei such as those studied here can be used for quantum computing without strongly perturbing their local environment. Reference 12 shows one possible architecture for quantum computing in nearly-pure, bulk crystalline silicon, motivating our measurements to explore limits in the coherence time of bulk ^{29}Si nuclei.

The qubit in this study is a thermal ensemble of N ^{29}Si nuclei, which are spin-1/2, in a single crystal of silicon. All other isotopes of silicon are spin-0. If the ^{29}Si nuclei were uncoupled and controlled by identical magnetic fields, the system would have only two accessible degenerate energy levels. However, the dipolar coupling lifts the degeneracy and takes superpositions of the two

TABLE I: Experimental Measurements of Coherence Times T_2 for Various Qubits. These times were all measured by spin-echo Ramsey spectroscopy or four-wave-mixing, except where noted. Q is the product of the fundamental qubit frequency $\omega_0/2\pi$ and πT_2 . The ΩT_2 column shows the experimental product of the Rabi frequency and the coherence time; this provides a more realistic measure than Q of the available number of sequential single-qubit gates. Technical improvements can increase ΩT_2 as far as Q in some architectures, while for others Ω must be limited in order to maintain selective qubit control. The JT_2 column shows the product of the coherence time and the measured or expected qubit-qubit coupling speed; roughly the available number of sequential two-qubit gates.

	Qubit	$\omega_0/2\pi$	T_2	Q	ΩT_2	JT_2	Ref.
Atomic	Trapped Optical Ions ($^{40}\text{Ca}^+$)	412 THz	1 ms	10^{12}	10^2	10^1-10^3	4
	Trapped Microwave Ions ($^9\text{Be}^+$)	1.25 GHz	1 ms	10^6	10^3	10^1-10^3	5
	Molecular Nuclei in Liquid Solution	500 MHz	2 sec	10^9	10^5	10^2	6
Solid-State	Charge States in Quantum Dots	200–600 THz	40–630 ps	10^5	10^2	10^2	7
	Josephson-Junction Flux Qubits	6.6 GHz	30 ns ^a	10^3	10^2	10^1	9
	Josephson-Junction Charge Qubits	16 GHz	500 ns	10^4	10^2	10^4	10
	Josephson-Junction Phase Qubits	16 GHz	5 μs ^b	10^5	10^1	10^4	11
	^{29}Si Nuclei in Solid Silicon	60 MHz	25 sec	10^9	10^6	10^4	12, ^c

^a A recent measurement employing continuous measurement of Rabi oscillations indicates a T_2 of 2.5 μs in this system [8].

^b This result used the decay of low-visibility Rabi oscillations.

^c As shown in this Letter.

qubit states into much larger, entangled superpositions of all the 2^N available states. These dynamics are nearly independent of temperature. The qubit information is not completely lost by this dipolar scrambling, since information only leaks from the 2^N nuclear states to the lattice on a timescale much slower than the dipolar dynamics. The quantum information can be “refocused” by decoupling pulse sequences such as WAHUHA [18] and its offspring, which periodically reverse the dipolar evolution, extending T_2 by several orders of magnitude.

The nuclear dynamics during such sequences are usually described using average Hamiltonian theory (AHT), in which the effects of the periodic RF field on the system Hamiltonian are expanded in powers of t_c , the sequence period [19]. The system Hamiltonian for a nuclear dipolar solid in the rotating frame may be written as

$$\mathcal{H} = - \sum_j \hbar \omega_j I_j^z - \sum_{jk} D_{jk} [\mathbf{I}_j \cdot \mathbf{I}_k - 3I_j^z I_k^z], \quad (1)$$

where \mathbf{I}_j is the spin vector and ω_j the shift of the Larmor frequency from the RF carrier for the j^{th} nucleus. The dipolar coupling coefficients are $D_{jk} = \hbar^2 \gamma^2 (1 - 3 \cos^2 \theta_{jk}) / 2r_{jk}^3$, where $r_{jk} \cos \theta_{jk} = (\mathbf{r}_j - \mathbf{r}_k) \cdot \hat{z}$. The values of ω_j and D_{jk} are different for each nucleus due to the inhomogeneous magnetic field and the random distribution of the ^{29}Si nuclei in the crystal lattice. The sequence we employ in this study consists of 16 properly phased and separated $\pi/2$ pulses, forming MREV-16, a variant of the MREV-8 sequence [20]. With perfect pulses, the MREV-8 sequence results in the zero-order average Hamiltonian $\mathcal{H}^{(0)} = -(1/3) \sum_j \hbar \omega_j (I_j^z \pm I_j^x)$, where the sign of the x -component of the effective field depends on the helicity of the sequence. The MREV-16 sequence, shown in Fig. 1, concatenates each helicity leading to $\mathcal{H}^{(0)} = -\sum_j (\hbar \omega_j / 3) I_j^z$. Although MREV-

16 has reduced spectroscopic resolution over MREV-8, maintaining the effective field in the z -direction allows easier nuclear control. The inhomogeneous offsets described by $\mathcal{H}^{(0)}$ cause static dephasing, which we periodically refocus by applying π -pulses every 120 cycles of MREV-16. We employ the Carr-Purcell-Meiboom-Gill (CPMG) phase convention to correct for π -pulse errors [21], as shown in Fig. 1. Such inserted pulses would likewise be employed in a NMR quantum computer for decoupling and recoupling of multiple dipolar-coupled qubits [22]. We note that the CPMG convention changes the sequence according to the initial phase of the nuclear qubit, which is incompatible with the memory of unknown or entangled quantum states. However, more complex NMR techniques such as composite pulses [23] are known to allow phase-independent pulse correction. The MREV-16 sequence and the observed T_2 times are otherwise independent of the initial nuclear phase.

The experiments were performed using a 7 T superconducting solenoid NMR magnet (Oxford) and a commercial NMR spectrometer (Tecmag) operating at 59.575 MHz. The probe was homemade, employing variable vacuum capacitors (Jennings) and high-power ceramic capacitors (HEC) to accommodate the pulse powers of approximately 700 W while still allowing flexible tuning for frequency and impedance matching as well as phase transient symmetrization. The RF was detuned about 120 Hz from the center of the nuclear resonance frequency. Pulsed spin locking [24] was observed when π -pulses were applied every 5-10 cycles and in spin-echo experiments without decoupling, but this effect diminished as the π -pulse frequency was reduced. Each echo time-series was taken in a single measurement after thermal equilibration for half to five times T_1 .

As shown in Fig. 1, this combined “CPMG-MREV-

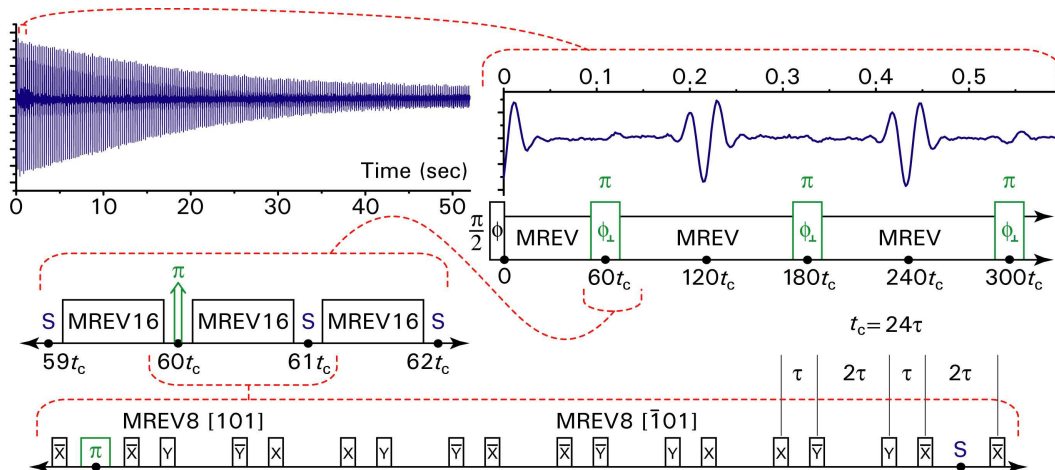


FIG. 1: Schematic of the CPMG-MREV-16 \times 120 pulse sequence. The echoes shown in the upper left and expanded in the upper right are data from an isotopically natural single crystal of silicon. These are obtained by first exciting the sample with a $\pi/2$ -pulse of arbitrary phase ϕ , decoupling with the MREV-16 sequence shown in detail on the bottom line, and refocussing with π -pulses of phase $\phi_{\perp} = \phi + \pi/2$ every 120 cycles of MREV-16. The magnetization is sampled once per MREV-16 cycle in the windows marked with an S.

16 \times 120" sequence allows the observation of hundreds of spin-echoes. In a cylindrical sample of single-crystal silicon with isotopic content 96.9% ^{29}Si , the T_2 due to unrefocussed dipolar-couplings is 450 μs for the $[001]$ orientation, as reported previously for this sample [25]. The CPMG-MREV-16 \times 120 sequence extends the coherence time in this sample to nearly 2 seconds. This experiment used a 6 cm-long, 1.5 cm coil wound using 2 mm-diameter wire with variable pitch to improve RF homogeneity. The $\pi/2$ -pulse duration was 9.6 μs for this coil. In isotopically natural silicon, the coherence time is even longer due to the scarcity of ^{29}Si in the lattice, as ^{29}Si is naturally only 4.7% abundant. We examined a high-quality single-crystal sample (Marketch) with less than $5 \times 10^{13} \text{ cm}^{-3}$ n -type impurities. It was cut into a sphere of diameter 1.5 cm and fit tightly in a constant-pitch coil approximately 6 cm long. The $\pi/2$ -pulse duration was 15 μs for this coil. As shown in Fig. 1, the spin-echoes in this sample last for as long as a minute, showing a T_2 of $25.0 \pm 0.2 \text{ sec}$.

MREV-16 is expected to reduce the effects of the dipolar coupling to second order in t_c by AHT, even in the presence of pulse errors [19]. Evidence for this order of reduction comes from the observation that T_2 increases quadratically as t_c is decreased (Fig. 2). The spin-echo data was analyzed by Fourier-transforming each echo and following the decay of the detuned side-peak, integrated between half-maxima. A center peak at the RF frequency usually appeared in the spectra due in part to ringdown effects and in part to nuclear spin-locking to an effective field, which tips slightly away from the z -axis in the presence of pulse imperfections. The least-squares fit to a single exponential was always used to extract the value of T_2 . The decrease in T_2 for small t_c occurs be-

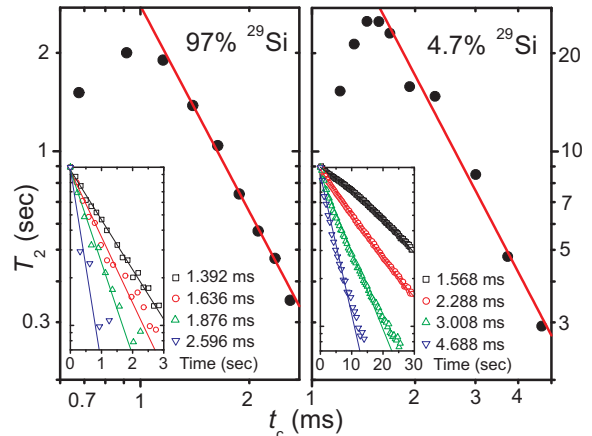


FIG. 2: Coherence time *vs.* cycle time. The solid line is a fit showing the exponent -2.09 ± 0.07 for the isotopically enhanced sample (left) and -2.00 ± 0.2 for the isotopically natural sample (right). The insets show the integrated log-magnitude of the spin-echoes decaying in time for a few cycle times.

cause MREV-16 begins to fail when the ratio of the pulse-width to the time τ between pulses approaches unity [19]. The maximum T_2 observed (25 sec) is not a fundamental result; it may be exceeded using higher-order pulse sequences or isotopic depletion.

As the strength of the dipolar coupling is further decreased by isotopic depletion, the dipolar coupling constants D_{jk} become much smaller than the frequency offsets ω_j . The dominant second-order dipolar average Hamiltonian term leading to decoherence is then the dipolar/offset cross term, which scales as $\mathcal{H}^{(2)} \propto t_c^2 |D_{jk}| |\omega_j^2|$. For isotopic percentage p less than about

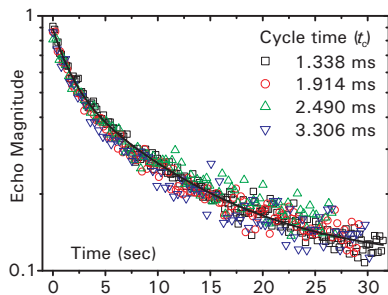


FIG. 3: Echo decay curves for pure polycrystalline silicon of natural isotopic abundance. The solid line is a fit to a double exponential with time constants 1.6 and 9.8 seconds. No significant variation in any timescale is observed as t_c is changed.

10%, we would expect T_2^{-1} to be proportional to the dipolar coupling constants, which vary as the inverse cube of the distance between ^{29}Si isotopes. Correspondingly, we expect $T_2^{-1} \propto p$, approaching T_1^{-1} as $p \rightarrow 0$, indicating that the threshold for fault-tolerant quantum computing could be obtained with reasonably depleted silicon.

We did observe another decoherence mechanism that could appear before the T_1 limit in real silicon crystals. In a polycrystalline sample with shallow impurity content similar to the single-crystal sample, we found the T_2 to be limited to a constant value of about 8 seconds, independent of t_c (Fig. 3). We also examined a p -type single crystal sample with roughly 1-1.5% ^{29}Si . This sample was known to contain a substantial number of dislocations in addition to $5 \times 10^{17} \text{ cm}^{-3}$ aluminum impurities. Although the data were noisy due to the reduced signal, T_2 was observed to be no longer than this same timescale of 8 seconds, even after 10-fold averaging.

We believe this reduced T_2 in polycrystalline silicon is due to the same low-frequency noise source that leads to $1/f$ noise in silicon wafers [26]. This noise is attributed to charge traps at lattice defects and other deep impurities, which lead to slow fluctuations of the diamagnetic shielding seen at nearby nuclei. Free carriers and fixed dipolar paramagnetic impurities are unlikely to be responsible for this T_2 , since these lead to isotropic magnetic noise with correlation times much shorter than the Larmor period. It follows that T_2 due to these sources would be on the same order of magnitude as T_1 , but we measured T_1 to be nearly 5 hours, consistent with earlier studies [27]. The elimination of $1/f$ noise from oxides and interfaces poses a critical fabrication challenge in quantum computing designs based on semiconductor impurities [16, 17] and Josephson junctions [9, 10, 11], but this noise is expected to be very small in high-quality bulk single-crystal silicon at low temperature.

Decoupling pulse sequences have been proposed for nuclear memory in high mobility GaAs/AlGaAs heterostructures [28]. We caution that the large RF power

required to effectively decouple the ubiquitous nuclear spins in this system may be inconsistent with millikelvin operation, even if small, high- Q coils and low power, windowless sequences [29] are employed. For this reason, we believe isotopically depleted silicon to be a more promising material for nuclear quantum memory, assuming that efficient methods for transferring quantum information to and from its well-isolated nuclei can be found.

This study was sponsored by the DARPA-QuIST program. T.D.L. was supported by the Fannie and John Hertz Foundation. We acknowledge N. Khaneja for useful discussions.

* Electronic address: tladd@stanford.edu

† Currently at Max-Planck-Institut für Festkörperforschung, D-70569, Stuttgart, Germany.

‡ Also at National Institute of Informatics, Tokyo, Japan.

- [1] M. A. Nielsen and I. L. Chuang, *Quantum Computation and Quantum Information* (Cambridge University Press, 2000).
- [2] P. Shor, Phys. Rev. A **52**, 2493 (1995); A.M. Steane, Phys. Rev. Lett. **77**, 793 (1996).
- [3] P. Shor, in *Proceedings, 37th Annual Symposium on Fundamentals of Computer Science* (IEEE Press, 1996), p. 56.
- [4] F. Schmidt-Kaler *et al.*, Nature **422**, 408 (2003); J. Phys. B: At. Mol. Opt. Phys. **36**, 623 (2003).
- [5] D. J. Wineland *et al.*, J. Res. Natl. Inst. Stand. Technol. **103**, 259 (1998); D. Liebfried *et al.*, Nature **422**, 412 (2003).
- [6] L. M. K. Vandersypen *et al.*, Nature **414**, 883 (2001).
- [7] N. H. Bonadeo *et al.*, Science **282**, 1473 (1998); M. Bayer *et al.*, *ibid.* **291**, 451 (2001); X. Li *et al.*, *ibid.* **301**, 809 (2003); P. Palinginis, S. Tavenner, M. Lonergan, and H. Wang, Phys. Rev. B **67**, 201307 (2003).
- [8] E. Il'ichev *et al.*, Phys. Rev. Lett. **91**, 097906 (2003).
- [9] J. E. Mooij *et al.*, Science **285**, 1036 (1999); I. Chiorescu, Y. Nakamura, C.J.P.M. Harmans, and J.E. Mooij, *ibid.* **299**, 1869 (2003).
- [10] Y. Makhlin, G. Schön, and A. Shnirman, Nature **398**, 305 (1999); Yu. A. Pashkin *et al.*, *ibid.* **421**, 823 (2003); D. Vion *et al.*, Science **296**, 886 (2002).
- [11] Y. Yu, S. Han, X. Chu, S-I. Chu, and Z. Wang, Science **296**, 889 (2002); A. J. Berkley *et al.*, *ibid.* **300**, 1548 (2003).
- [12] T.D. Ladd *et al.*, Phys. Rev. Lett. **89**, 17901 (2002).
- [13] S. Gulde *et al.*, Nature **421**, 48 (2003).
- [14] A. Tyryshkin, S. A. Lyon, A. V. Astashkin, and A. M. Raitsimring (2003), cond-mat/0303006.
- [15] D. Loss and D. DiVincenzo, Phys. Rev. A **57**, 120 (1998).
- [16] R. Vrijen *et al.*, Phys. Rev. A **62**, 012306 (2000).
- [17] B. Kane, Nature **393**, 133 (1998).
- [18] J. S. Waugh, L. M. Huber, and U. Haerberlin, Phys. Rev. Lett. **20**, 180 (1968).
- [19] M. Mehring, *Principles of High Resolution NMR in Solids* (Springer-Verlag, 1983).
- [20] P. Mansfield, M. J. Orchard, D. C. Stalker, and K. H. B. Richards, Phys. Rev. B **7**, 90 (1973); W-K. Rhim, D. D. Elleman, and R. W. Vaughan, J. Chem. Physics **59**,

- 3740 (1973).
- [21] S. Meiboom and D. Gill, *Rev. Sci. Instrum.* **29**, 6881 (1958).
- [22] D. W. Leung, I. L. Chuang, F. Yamaguchi, and Y. Yamamoto, *Phys. Rev. A* **61**, 042310 (2000).
- [23] M. H. Levitt and R. Freeman, *J. Magn. Reson.* **43**, 65 (1981).
- [24] E. D. Ostroff and J. S. Waugh, *Phys. Rev. Lett.* **16**, 1097 (1966); D. Suwelack and J. S. Waugh, *Phys. Rev. B* **22**, 5110 (1980).
- [25] A. Verhulst, D. Maryenko, Y. Yamamoto, and K. M. Itoh, *Phys. Rev. B* **68**, 054105 (2003).
- [26] R. D. Black, M. B. Weissman, and P. J. Restle, *J. Appl. Phys.* **53**, 6280 (1982); *Phys. Rev. B* **28**, 1935 (1983).
- [27] R. G. Shulman and B. J. Wyluda, *Phys. Rev.* **103**, 1127 (1956); G. Lampel and I. Solomon, *C. R. Acad. Sc. Paris* **258**, 2289 (1964); B. Sapoval and D. Lepine, *J. Phys. Chem. Solids* **27**, 115 (1966).
- [28] J. M. Taylor, C. M. Marcus, and M. D. Lukin, *Phys. Rev. Lett.* **90**, 206803 (2003).
- [29] D. Burum, M. Linder, and R. Ernst, *J. Magn. Reson.* **44**, 173 (1981).